Journal of Hepatocellular Carcinoma

Dovepress

open access to scientific and medical research

Open Access Full Text Article

ORIGINAL RESEARCH

PET Imaging of Hepatocellular Carcinoma Using ZD2-(^{68}Ga-NOTA)

Olga Sergeeva[1], Yifan Zhang[1], Songqi Gao[2], E Ricky Chan[3], Maxim Sergeev[4], Renuka Iyer[5], Sandra Sexton[5], Norbert Avril[4], Zheng-Rong Lu[2], Zhenghong Lee[1]

[1]Department of Radiology, Case Western Reserve University, Cleveland, OH, USA; [2]Department of Biomedical Engineering, Case Western Reserve University, Cleveland, OH, USA; [3]Cleveland Institute for Computational Biology, Case Western Reserve University, Cleveland, OH, USA; [4]Department of Radiology, University Hospitals Cleveland Medical Center, Cleveland, OH, USA; [5]Medical Oncology and Laboratory Animal Shared Resources, Roswell Park Cancer Institute, Buffalo, NY, USA

Correspondence: Zhenghong Lee, Nuclear Medicine, Radiology, Case Western Reserve University, Bolwell S107, 11100 Euclid Avenue, Cleveland, OH, 44106, USA, Tel +1216-844-7920, Email zxl11@case.edu; Zheng-Rong Lu, Biomedical Engineering, Case Western Reserve University, Wickenden 427, Mail Stop 7207, 10900 Euclid Ave, Cleveland, OH, 44106, USA, Tel +1 216-368-0187, Email zxl125@case.edu

Purpose: We tested a recently developed short peptide radioligand for PET imaging of hepatocellular carcinoma (HCC) by targeting an oncoprotein, extra-domain B fibronectin (EDB-FN) in the tumor microenvironment.

Methods: The radioligand consists of a small linear peptide ZD2 with ^{68}Ga-NOTA chelator, and specifically binds to EDB-FN. PET images were acquired dynamically for 1 hour after intravenously (i.v.) injecting 37 MBq (1.0 mCi) of the radioligand into the woodchuck model of naturally occurring HCC. Woodchuck HCC originated from chronic viral hepatitis infection, which recapitulates the corresponding human primary liver cancer. The animals were euthanized post-imaging for tissue collection and validation.

Results: For ZD2 avid liver tumors, the radioligand accumulation plateaued a few minutes after injection, while the liver background uptake stabilized 20 min post-injection. The status of EDB-FN in woodchuck HCC was confirmed by histology and validated by PCR and western blocking.

Conclusion: We have showed the viability of using the ZD2 short peptide radioligand targeting EDB-FN in liver tumor tissue for PET imaging of HCC, which can potentially impact the clinical care for HCC patients.

Keywords: peptide ligand, EDB fibronectin, positron emission tomography, woodchuck model

Introduction

Primary liver cancer hepatocellular carcinoma (HCC) is one of the leading causes of cancer-related death worldwide with increasing incidence and mortality.[1] Currently, clinical diagnosis of HCC depends heavily on imaging with contrast-enhanced CT or MRI angiography to detect a signature vascular flow pattern.[2] Yet, some primary liver cancer do not show the "typical" vascular flow pattern.[3] A significant limitation of these traditional size-based or flow-based imaging measurements is that they did not characterize biological aspect(s) of liver cancer and are, therefore, sometimes supplemented by biopsies for subsequent histopathology analysis. Positron Emission Tomography (PET) offers molecular and cellular information if an appropriate PET imaging biomarker exists. The clinically used PET radiotracer, 2-[^{18}F]-fluoro-2-deoxy-D-glucose (FDG) depicts increased cellular glucose metabolism and has dramatically impacted patient management with a large variety of cancers. However, we and others discovered that FDG has certain limitations for imaging primary liver cancers such as HCC due to a relatively lower FDG uptake leading to high false-negative rate.[4] Many other PET ligands typically exhibit a high background uptake in the liver, which can interfere with the detection of liver cancer.

The short peptide ZD2 (Thr-Val-Arg-Thr-Ser-Ala-Asp) specifically binds to the extra-domain B fibronectin (EDB-FN, expressed by FN1 gene),[5] and was initially developed for imaging prostate,[6] breast[7] and pancreatic cancers.[8] We investigated this novel short peptide for radiolabeling with Gallium-68 (^{68}Ga) via 1,4,7-triazacyclononane-1,4,7-triacetic

Received: 10 October 2022
Accepted: 14 February 2023
Published: 22 February 2023

acid (NOTA) chelator into ZD2-(^{68}Ga-NOTA), for PET imaging of HCC. EDB-FN being an oncofetal isoform of fibronectin is abundant in the extracellular matrix (ECM) and perivascular space of various aggressive cancers, but absent in normal tissues.[9,10] Fibronectin, including its oncofetal subtype EDB-FN, is a hall marker of epithelial-to-mesenchymal transition (EMT), a process associated with drug resistance and metastatic invasion in aggressive cancers.[11–14] High EDB-FN expression in primary cancers is correlated with a high incidence of metastasis and poor overall survival of patients diagnosed with pancreatic, prostate, breast, ovarian, and head and neck cancer.[15–19] Clinical evidence has demonstrated that oncofetal fibronectin (FN1) is highly expressed in invasive cancers.[20–26] The Cancer Genome Atlas (TCGA) data confirmed the high expression of EDB-FN in human HCC, which is inversely associated with patient survival.

We tested ZD2-(^{68}Ga-NOTA) for quantitative PET imaging of malignant liver cancer with an animal model of clinical relevance, the naturally occurring HCC in woodchucks. The animal model (eastern woodchuck, *Marmota monax*) develops HCC after chronic viral hepatitis infection when it harbors a DNA virus – the woodchuck hepatitis virus (WHV),[27] a member of the family Hepadnaviridae, of which human hepatitis B virus (HBV) is the prototype. Analogous to HBV, WHV infects woodchuck liver to cause acute and chronic hepatitis, leading to the development of HCC within 2–4 years of life. We have established the value of this animal model for enabling the development and characterization for a list of PET radioligands.[28–31] The protein sequence of the EDB fragment is conserved among the species, and the woodchucks' EDB-FN is homologous to the humans'.

Materials and Methods

Woodchuck Model of Naturally Occurring HCC

Three woodchucks (2 males: WC#1701 and WC#1741 and 1 female: WC#1857) of 8–10 lbs (averaged 3.5 kg) body weight were ultrasound-screened at Roswell Park Comprehensive Cancer Center (Buffalo, NY), selected and shipped to Case Western Reserve University (Cleveland, OH) when their liver nodules were ≥20 millimeters measured along the long-axis. The veterinarian at Roswell Park Cancer Center surgically implanted a venous access port (SAI Infusion Technologies; Elgin, IL) in each animal before shipment to us in Cleveland to facilitate intravenous (i.v.) administration of the radiotracer for PET imaging. The port was flushed regularly with heparinized saline. The food was taken away 4–5 hours before each PET imaging to facilitate the anesthesia procedure while drinking water was kept accessible. All procedures were approved by the Institutional Animal Care and Use Committee (IACUC) of the University.

Bioinformatics

As reported previously, TCGA data were downloaded from the public TCGA Liver Hepatocellular Carcinoma database (TCGA-LIHC) and processed as previously reported.[32,33] The woodchuck data were collected from the NCBI Gene Expression Omnibus (accession number GSE36545 and BioProject PRJNA155585). The data include 102 samples (GSM896624-GSM896725) from 13 woodchucks with a total of 42 tumor samples and 60 non-tumor samples.[34] The data obtained were from a custom NimbleGen Woodchuck Gene Expression HX3 Microarray and formatted in parallel to the TCGA dataset, although the two sets of data were processed differently due to the difference in the dynamic range inherent to each technology.[32,33]

The expression of FN1 between liver tumors and non-tumor liver tissues was tallied from the databases. The human data came from TCGA, and the woodchuck data from the customized microarray. Homology of amino acid sequences between human ([Homo sapiens]) and woodchuck ([marmot]) EDB-FN was determined by using Protein Basic Local Alignment Search Tool (BLAST) (https://blast.ncbi.nlm.nih.gov/Blast.cgi).

Synthesis of Radiolabeled ZD2-[^{68}Ga-NOTA]

The radiosynthesis of ZD2-[^{68}Ga-NOTA] was performed in closed-system fully automated Scintomics GRP® synthesizer (Furstenfeldbruck, Germany) as reported previously.[8] Briefly, ^{68}Ge/^{68}Ga generator (model IGG-100) was used as a source of radionuclide. In the process of automated synthesis, ^{68}Ga(III) was eluted from a generator with 0.1 M hydrochloric acid, and the eluent was diluted with water. The resulting solution was passed through the cationic

exchange PS-H+ cartridge and subsequently eluted with 5 M sodium chloride solution into a pre-heated reactor containing ZD2-NOTA and HEPES buffer. The labeling was performed in 10 min at 125°C. After reaction, the reaction content was transferred onto C18 Plus Light SPE-cartridge, and the labeled ZD2-(^{68}Ga-NOTA) was eluted with a mixture of water for injection/ethanol (1/1, v/v) through the 0.22 μm membrane sterile filter into the final product vial. Finally, the product was diluted with a PBS buffer through the same sterile 0.22 μm membrane filter into the final product vial. Samples are then aseptically removed for quality control testing.

PET Imaging and Data Analysis

Woodchucks with an average weight of 3.5 kg were too large to fit into our microPET scanner and were placed prone in our clinical Ingenuity PET/CT scanner (Philips, Cleveland, OH) instead. Under 3% isoflurane gas anesthesia, the animals had a low-dose CT scan first, followed by i.v. injection of 37 ~ 56 MBq (1.0 ~ 1.5 mCi) ZD2-(^{68}Ga-NOTA) via the implanted venous access port. A dynamic PET acquisition in list mode started upon injection and lasted 60 min. The PET acquisition was re-binned into a total of 21 frames: 10×30 seconds, 5 X 1-min, 2 X 5-min frames, and 4×10 min, respectively, and reconstructed using iterative 3D-OSEM provided by the vendor incorporating the built-in CT-based attenuation correction. After the scan, the animals were euthanized for tissue harvesting including tumor and matched liver tissues. Some samples were fresh-frozen immediately for later use in PCR or Western blot, while others were fixed with formaldehyde for histology.

Standardized Uptake Value (SUV, normalized radiotracer uptake by body weight and injected tracer dose)[35] was calculated for regions of interest (ROIs) defined over focal uptakes of the ZD2 ligand as well as a nearby ROI over the liver background away from focal uptakes, similar to that used for computing FDG uptake.[36] Time activity curves in the unit of SUV were generated for these ROIs.

EDB-FN Expression (PCR and Western Blot)

RNA was extracted from previously frozen tissue using Qiagen miRNeasy Mini Kit (Qiagen) according to manufacturer's instructions. The primers for qRT-PCR were designed at The Custom TaqMan® Assay Design Tool based on human mRNA sequences for required genes: EDB-FN (custom TaqMan gene expression assay AP47XKP), and endogenous control gene GAPDH (assay Hs02758991_g1). qRT-PCR was performed on a StepOne Plus real-time thermocycler with 1.33 mL of cDNA for each reaction and the TaqMan Universal Master Mix II with UNG (Applied Biosystems). Expression data was processed similarly as before.[32,33,37] The relative quantification of gene expression (RQ) for the reference sample was set as 1.

The same frozen liver tissues used for PCR above were thawed and processed for Western blotting in a similar fashion as before[32,33,37] but with the primary antibody specific to EDB-FN (G4, Abcam, Cambridge, MA). The blot was incubated with an HRP-conjugated secondary antibody and then treated with a chemiluminescent ECL reagent before development. ß-actin in the tissue specimens was used as a reference protein. The blots were washed in TBST and developed with ECL Chemiluminescent detection reagent (Cytiva Amersham™). Chemiluminescence signals were visualized using the exposure film.

Histology

Fixed tissue samples embedded in the paraffin blocks were cut, and the histological sections were deparaffinized in xylene, ethanol, and tap water washes, and then blocked with 10% goat serum (Invitrogen, Carlsbad, CA) in PBS with 0.1% Tween 20 (PBS-T) (Gibco, Waltham, MA) for 30 min. The staining of the tissue slides was performed with a commercial antibody specific to EDB-FN (G4, Abcam). In addition, the tissue slides were incubated with ZD2-Cy5.5 (500 nM) in PBS-T for 1 hour. Following three washes with PBS-T, the sections were mounted using fluoroshield mounting medium with DAPI (Abcam, Cambridge, UK). Images were acquired on a confocal microscope using pre-programmed emission and excitation filters for Cy5.5 (635 nm excitation, 693 nm emission) (Olympus, Tokyo, Japan) and DAPI (405 nm excitation, 461 nm emission).

Results

ZD2-[^{68}Ga-NOTA]

The radioactive tracer ZD2-[^{68}Ga-NOTA] was synthesized under the standard GMP conditions. The typical decay-corrected radio-chemical yield (d.c. RCY) is ~71% (~54% n.d.c. RCY at EOS).

Quality control tests similar to those for clinical formulations of [^{68}Ga]Ga-labeled peptides showed that the product solution was colorless without particles, pH = 7.0, endotoxin test <2 EU/mL, radiochemical purity >90% as show by HPLC (C18 RP column, 0.1% TFA/H_2O – 0.1% TFA/ACN). The average specific activity was ~6 Ci/μmol. Stability studies over the course of 3 hours did not reveal any product degradation, and radiochemical purity remained the same on all test chromatograms.

Bioinformatics

The protein sequence of the EDB fragment is conserved in all mammalian species as confirmed by BLAST for the woodchucks whose EDB-FN sequence is 100% homology to the humans, as shown in Table 1. TCGA Liver Statistic revealed (http://cancergenome.nih.gov) an averaged RPKM (Reads Per Kilobase of transcript, per Million mapped reads, a normalized unit for mRNA expression) of 8.7 for FN1 mRNA in liver cancer as compared to an averaged RPKM of 1.8 in liver parenchyma. High expression of EDB-FN in HCC is associated with a disadvantage in patient survival (https://portal.gdc.cancer.gov/projects/TCGA-LIHC), Figure 1. In comparison, the analysis of the customized microarray data also showed a higher EDB-FN expression in the woodchuck HCC comparing to the surrounding hepatic tissues (Figure 2A).

PET Imaging of HCC with ZD2-[^{68}Ga-NOTA]

PET imaging revealed a higher uptake of ZD2-[^{68}Ga-NOTA] in woodchuck HCC than that in normal tissues and organs including liver, kidney, spleen, and muscle. Figure 3 shows an exemplary animal with HCC, which displayed a high uptake in one HCC the along with a rapid renal clearance indicating that the tracer was mainly excreted via renal filtration. The accumulation of ZD2-[^{68}Ga-NOTA] in HCC plateaued 10 min after injection and the liver background uptake stabilized 20 min post-injection. PET images of other animals and the accompanying time activity curves for their ROIs (Figures S1–S4) are presented in the Supplemental Information.

Histology

EDB-FN expression was also determined in the tumor sections using immunofluorescence staining with G4 anti-EDB-FN monoclonal antibody.[38] As shown in Figure 4A, substantial expression of EDB-FN was observed in HCC, while no expression was observed in normal liver, consistent with the reported results in other cancers.[39] The high expression of EDB-FN was mainly observed in the extracellular matrix of the HCC.

Specific binding of ZD2 peptide to EDB-FN in HCC was tested by incubating ZD2-Cy5.5 with the tumor sections. As shown in Figure 4B, strong binding of ZD2-Cy5.5 (red) was observed in tumor tissues, similar to the immunofluorescence staining in Figure 4A. Little fluorescence staining was observed for the HCC specimens pre-incubated with G4 antibody and followed by ZD2-Cy5.5, indicating blockage of ZD2-Cy5.5 binding by G4 antibody (blocking). The results suggest that both ZD2-Cy5.5 and G4 specifically bind to the same EDB-FN protein target in the tumor tissues. Taken together, ZD2 peptide is a promising targeting agent for specific binding of EDB-FN in HCC.

Table 1 BLAST of EDB-FN Amino Acid Sequence Showing 100% Homology Between Human and Woodchuck

Human 1	EVPQLTDLSFVDITDSSIGLRWTPLNSSTIIGYRITVVAAGEGIPIFEDFVDSSLGYYTV	60
	EVPQLTDLSFVDITDSSIGLRWTPLNSSTIIGYRITVVAAGEGIPIFEDFVDSSLGYYTV	
Marmot 1267	EVPQLTDLSFVDITDSSIGLRWTPLNSSTIIGYRITVVAAGEGIPIFEDFVDSSLGYYTV	1326
Human 61	TGLEPGIDYDISVITLINGGESAPTTLTQQT	91
	TGLEPGIDYDISVITLINGGESAPTTLTQQT	
Marmot 1327	TGLEPGIDYDISVITLINGGESAPTTLTQQT	1357

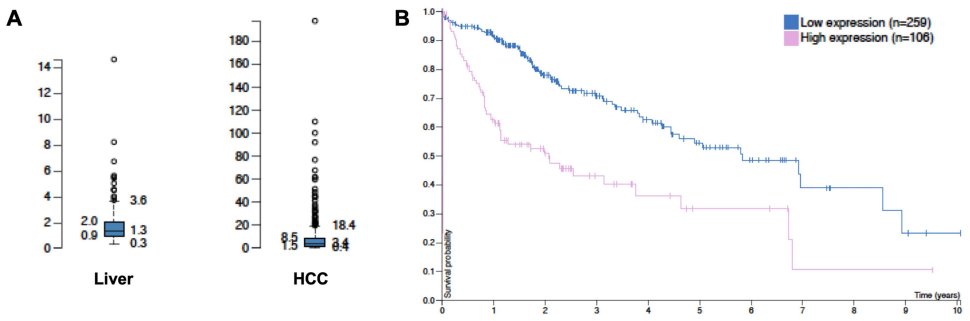

Figure 1 TCGA data showing higher EDB-FN expression in HCC compared with that in the liver (**A**), and the inverse correlation of EDB-FN expression in HCC with patient survival (**B**).

Expression of EDB-FN

The expression of EDB-FN was also determined in harvested tissue samples from the woodchucks carrying HCC with RT-PCR (Figure 2B) and Western blotting (Figure 2C). The results indicate that EDB-FN is highly expressed in the woodchuck HCC. In comparison, according to human Protein Atlas (https://www.proteinatlas.org/ENSG00000115414-FN1), FN1 gene mRNA expression is high in the lung, liver, and placenta tissues in that order. However, protein levels are high in kidney and placenta, while moderate to low in other organs (cerebellum, adrenal glands, lungs, etc.). The level of FN1 protein in the liver is low.

Discussion

Currently, standard radiological imaging (CT or MRI) supplemented with histopathological evaluation following tissue biopsy is the mainstay diagnostic approach for the detection and diagnosis of HCC. These conventional clinical imaging modalities could be improved by using PET imaging if a suitable PET imaging biomarker exists. We have successfully examined a long list of small molecular PET radioligands with a clinically relevant animal model of HCC in woodchucks to validate the corresponding findings in a clinical setting regarding radiotracer uptake mechanisms.[28–31,40–46]

EDB-FN (FN1), an oncofetal isoform of fibronectin, which is abundant in ECM and perivascular space of tumor microenvironment, is assembled by stromal cells such as cancer-associated fibroblasts (CAFs, or tumor-associated fibroblasts: TAFs),[47,48] linking to high malignancy and poor prognosis, while benign tumors have little or no presence of the protein.[19,22] As discussed below, one of the cell surface markers of these CAFs or TAFs used for targeting was the fibroblast activated protein (FAP),[49] which is not our target. Strong expression of EDB-FN in primary tumors is correlated with a high incidence of metastasis and poor overall survival of patients diagnosed with pancreatic, prostate, breast, ovarian, and head and neck cancer. TCGA (http://cancergenome.nih.gov) data demonstrated that EDB-FN is also highly expressed in HCC and is inversely correlated with patient survival (Figure 1).

Monoclonal antibodies have been developed to specifically target EDB-FN in cancer. Imaging probes have been developed and tested in kind using some antibodies or their fragments such as L19 targeting EDB-FN.[50,51] Because of their large size and long circulation time, a lengthy waiting time is required for the clearance of unbound antibody-derived radiotracers from the circulation and background for better cancer imaging, which is not convenient for both the patients and clinicians. ZD2, a seven-amino acid peptide, was selected for radiolabeling and PET imaging in this project due to its high appearance frequency during phage display and water solubility suitable to be a PET tracer, which are advantageous features for minimizing non-specific tissue binding. The affinity was measured at 132 nM, which is in accord with the predicted affinity to EDB-FN investigated with AutoDock Vina.[52] ZD2 did not bind to any cell surface target(s), rather to the abundant onco-fibronectin in the tumor microenvironment. Due to this amplification, radiolabeled ZD2 with a modest binding affinity directly depicted EDB-FN distribution associated with the tumor during PET imaging. This is different from the recently developed FAP inhibitor (FAPi)-based radioligands,[53,54] which target the FAP on cell surface of CAFs or TAFs. The ZD2 ligand was synthesized using standard solid-phase peptide chemistry and chelated to ^{68}Ga as a small molecular PET probe ZD2-(^{68}Ga-NOTA) prior to imaging. The radiosynthesis was performed

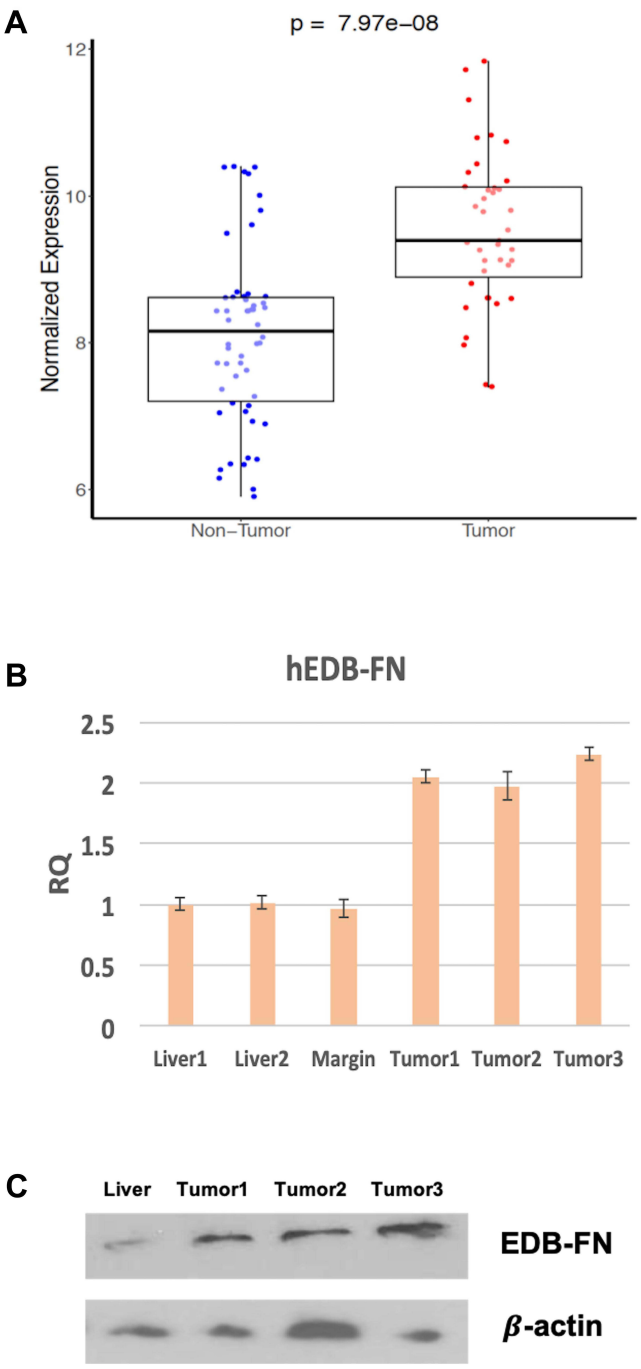

Figure 2 Validation results indicating highly expressed EDB-FN in the woodchuck HCC. (**A**) Higher EDB-FN expression in the woodchuck HCC compared to the surrounding hepatic tissues analyzed from the customized microarray data; Higher EDB-FN expression in HCC compared to the surrounding liver determined in harvested tissue samples from the woodchucks carrying HCC with RT-PCR (**B**) and Western blotting (**C**).

with the existing GMP facility for clinical Ga-68 tracers with a high yield and purity. The peptide and ZD2-(^{68}Ga-NOTA) are highly water-soluble. The small size and water solubility allow rapid diffusion of ZD2-(^{68}Ga-NOTA) into tumor tissues, thereby effectively binding to EDB-FN in the tumor ECM. Its high hydrophilicity would also minimize non-specific interactions with normal tissues, including the liver, and allow quick clearance via renal filtration for timely and efficacious diagnostic imaging, as shown in Figure 3.

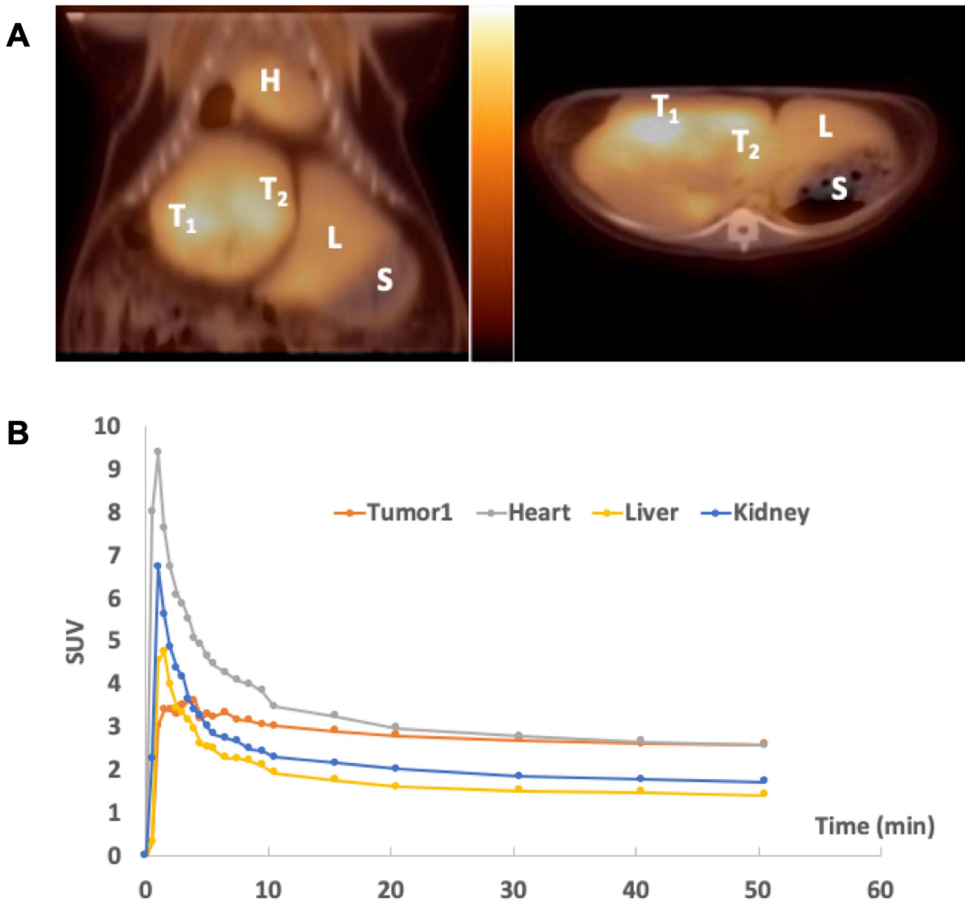

Figure 3 PET imaging of ZD2-[^{68}Ga-NOTA] with woodchuck (#1701). (**A**) PET/CT overlays of coronal (left) and axial (right) cuts showing uptake in one HCC (T_1 for tumor 1) with L for liver, S for stomach, and H for heart; (**B**) region-based uptake (in SUVs) as time activity curves for these organs.

Our long-term goal is to develop molecular PET imaging of EDB-FN, which has the potential to provide non-invasive and accurate diagnosis and risk-stratification of HCC to supplement standard clinical imaging such as ultrasound, contrast-enhanced multi-phase CT, and MR scans. This project started to characterize EDB-FN expression in a clinically relevant animal model of HCC in woodchucks and performed quantitative PET imaging analyses for assessing the potential of the EDB-FN-targeting peptide for future clinical translation. EDB-FN is highly conserved between species (Table 1). Our preliminary PET imaging studies using this spontaneous woodchuck model of HCC clearly displayed a high tumor uptake of the EDB-FN-targeting peptide labeled with ^{68}Ga, while showing a rapid liver background washout. The animal model came with a level of hepatic fibrosis (which contributed to liver background uptake) leading to the development of HCC but did not manifest to the degree of clinical cirrhosis. Conversely, cirrhosis is also absent in a sub-population of HCC patients with chronic HBV.[55] The HCC in woodchucks is thus valuable recapitulating the human HCC with similar pathology and natural history.[27,56]

Accurate determination of EDB-FN expression in tumor microenvironment is critical for distinction of aggressive HCC to assist decision-making in patient care. Furthermore, patients with liver cancer often carry other underlying liver or non-liver sickness such as cardiovascular diseases, or digestive disorders, or neural-brain illness. Identifying aggressive HCCs will help risk-stratification for prioritizing overall treatment plans. Future efforts will be directed towards clinical translation to establish oncofetal protein EDB-FN as a new target and ZD2-[^{68}Ga-NOTA] as the matching radioligand for PET imaging of primary liver cancers to supplement standard clinical scans and to reduce the need of liver biopsies.

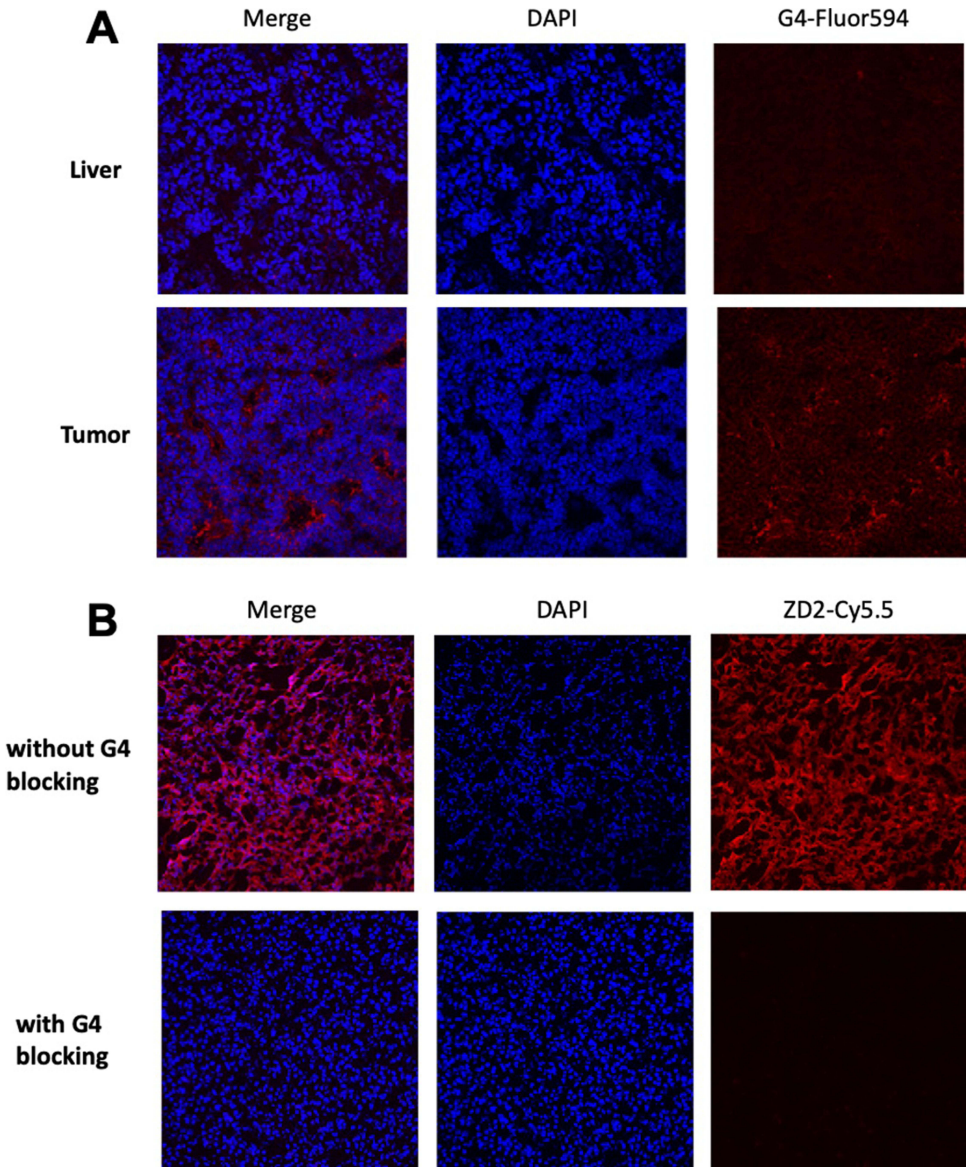

Figure 4 Histology analysis. (**A**) Immunofluorescence staining of woodchuck frozen sections (upper: liver, lower: tumor) with G4 anti-EDB-FN monoclonal antibody (red). While substantial EDB-FN was stained in the extracellular matrix of the HCC, normal liver was not stained; (**B**) Specific binding of ZD2 peptide to EDB-FN in woodchuck HCC was observed for strong binding of ZD2-Cy5.5 (red) in tumor tissues while little fluorescence staining was observed for the adjacent woodchuck HCC sections pre-incubated with G4 antibody and followed by ZD2-Cy5.5, indicating blockage of ZD2-Cy5.5 binding by G4 antibody (blocking).

Conclusion

Our results revealed that EDB-FN as an oncoprotein is a molecular target for sensitive imaging of HCC. The ZD2 short peptide radioligand targeting EDB-FN in liver cancer microenvironment seemed suitable for PET imaging of HCC. This will potentially impact the clinical management of patients with HCC.

Acknowledgments

This study was supported in part by National Institutes of Health (NIH) R01CA204373, R01CA211762, and R01CA235152, and by the Clinical and Translational Science Collaborative of Cleveland, UL1TR002548 from the National Center for Advancing Translational Sciences (NCATS) component of the NIH and NIH Roadmap for Medical Research. Its contents are solely the responsibility of the authors and do not necessarily represent the official views of the NIH. All experimental procedures were approved by the Institutional Animal Care and Use Committee and Radiation

Safety Committee at Case Western Reserve University (Cleveland, OH) and followed guidelines of US Department of Agriculture Animal Welfare Act, Public Health Service Policy on Humane Care and Use of Laboratory Animals, and Association for Assessment and Accreditation of Laboratory Animal Care International.

Disclosure

Dr Songqi Gao reports a patent WO2020150617A8 licensed to CWRU. Dr Zheng-Rong Lu reports a patent US Patent App. 17/424,104 pending to Molecular Theranostics, LLC. The authors report no other conflicts of interest in this work.

References

1. NIH. *Action Plan for Liver Disease Research: A Report of the Liver Disease Subcommittee of the Digestive Diseases Interagency Coordinating Committee*. NIH Publication; 2004.
2. Bruix J, Sherman M. Practice guidelines committee AAftSoLD. management of hepatocellular carcinoma. *Hepatology*. 2005;42(5):1208–1236. doi:10.1002/hep.20933
3. Lee JH, Lee JM, Kim SJ, et al. Enhancement patterns of hepatocellular carcinomas on multiphasic multidetector row CT: comparison with pathological differentiation. *Br J Radiol*. 2012;85(1017):e573–e583. doi:10.1259/bjr/86767895
4. Jeng LB, Changlai SP, Shen YY, Lin CC, Tsai CH, Kao CH. Limited value of 18F-2-deoxyglucose positron emission tomography to detect hepatocellular carcinoma in hepatitis B virus carriers. *Hepato-Gastroenterology*. 2003;50(54):2154–2156.
5. Han Z, Zhou Z, Shi X, et al. EDB fibronectin specific peptide for prostate cancer targeting. *Bioconjug Chem*. 2015;26(5):830–838. doi:10.1021/acs.bioconjchem.5b00178
6. Han Z, Sergeeva O, Roelle S, et al. Preparation and evaluation of ZD2 Peptide (64) Cu-DOTAConjugate as a positron emission tomography probe for detection and characterization of prostate cancer. *ACS Omega*. 2019;4(1):1185–1190.
7. Ayat NR, Vaidya A, Yeung GA, et al. Effective MR molecular imaging of triple negative breast cancer with an EDB-fibronectin-specific contrast agent at reduced doses. *Front Oncol*. 2019;9:1351.
8. Gao S, Qin J, Sergeeva O, et al. Synthesis and assessment of ZD2-((68) Ga-NOTA)specific to extradomain B fibronectin in tumor microenvironment for PET imaging of pancreatic cancer. *Am J Nucl Med Mol Imaging*. 2019;9(5):216–229.
9. Sauer S, Erba PA, Petrini M, et al. Expression of the oncofetal ED-B-containing fibronectin isoform in hematologic tumors enables ED-B-targeted 131I-L19SIP radioimmunotherapy in Hodgkin lymphoma patients. *Blood*. 2009;113(10):2265–2274.
10. Wagner K, Schulz P, Scholz A, Wiedenmann B, Menrad A. The targeted immunocytokine L19-IL2 efficiently inhibits the growth of orthotopic pancreatic cancer. *Clin Cancer Res*. 2008;14(15):4951–4960. doi:10.1158/1078-0432.CCR-08-0157
11. Antoon JW, Lai R, Struckhoff AP, et al. Altered death receptor signaling promotes epithelial-to-mesenchymal transition and acquired chemoresistance. *Sci Rep*. 2012;2:539. doi:10.1038/srep00539
12. Wang R, Cheng L, Xia J, Wang Z, Wu Q, Wang Z. Gemcitabine resistance is associated with epithelial-mesenchymal transition and induction of HIF-1alpha in pancreatic cancer cells. *Curr Cancer Drug Targets*. 2014;14(4):407–417. doi:10.2174/1568009614666140226114015
13. Parvani JG, Gujrati MD, Mack MA, Schiemann WP, Lu ZR. Silencing beta3 integrin by targeted ECO/siRNA nanoparticles inhibits EMT and metastasis of triple-negative breast cancer. *Cancer Res*. 2015;75(11):2316–2325. doi:10.1158/0008-5472.CAN-14-3485
14. Vaidya A, Wang H, Qian V, Gilmore H, Lu ZR. Overexpression of extradomain-B fibronectin is associated with invasion of breast cancer cells. *Cells*. 2020;9(8):1826.
15. Vaidya A, Ayat N, Buford M, et al. Noninvasive assessment and therapeutic monitoring of drug-resistant colorectal cancer by MR molecular imaging of extradomain-B fibronectin. *Theranostics*. 2020;10(24):11127–11143. doi:10.7150/thno.47448
16. Hesse E, Musholt PB, Potter E, et al. Oncofoetal fibronectin--a tumour-specific marker in detecting minimal residual disease in differentiated thyroid carcinoma. *Br J Cancer*. 2005;93(5):565–570. doi:10.1038/sj.bjc.6602741
17. Kaspar M, Zardi L, Neri D. Fibronectin as target for tumor therapy. *Int J Cancer*. 2006;118(6):1331–1339. doi:10.1002/ijc.21677
18. Mhawech P, Dulguerov P, Assaly M, Ares C, Allal AS. EB-D fibronectin expression in squamous cell carcinoma of the head and neck. *Oral Oncol*. 2005;41(1):82–88. doi:10.1016/j.oraloncology.2004.07.003
19. Richter P, Junker K, Franz M, et al. IIICS de novo glycosylated fibronectin as a marker for invasiveness in urothelial carcinoma of the urinary bladder (UBC). *J Cancer Res Clin Oncol*. 2008;134(10):1059–1065. doi:10.1007/s00432-008-0390-6
20. Santimaria M, Moscatelli G, Viale GL, et al. Immunoscintigraphic detection of the ED-B domain of fibronectin, a marker of angiogenesis, in patients with cancer. *Clin Cancer Res*. 2003;9(2):571–579.
21. Kaczmarek J, Castellani P, Nicolo G, Spina B, Allemanni G, Zardi L. Distribution of oncofetal fibronectin isoforms in normal, hyperplastic and neoplastic human breast tissues. *Int J Cancer*. 1994;59(1):11–16. doi:10.1002/ijc.2910590104
22. Nam JM, Onodera Y, Bissell MJ, Park CC. Breast cancer cells in three-dimensional culture display an enhanced radioresponse after coordinate targeting of integrin alpha5beta1 and fibronectin. *Cancer Res*. 2010;70(13):5238–5248. doi:10.1158/0008-5472.CAN-09-2319
23. Loridon-Rosa B, Vielh P, Matsuura H, Clausen H, Cuadrado C, Burtin P. Distribution of oncofetal fibronectin in human mammary tumors: immunofluorescence study on histological sections. *Cancer Res*. 1990;50(5):1608–1612.
24. Koukoulis GK, Howeedy AA, Korhonen M, Virtanen I, Gould VE. Distribution of tenascin, cellular fibronectins and integrins in the normal, hyperplastic and neoplastic breast. *J Submicrosc Cytol Pathol*. 1993;25(2):285–295.
25. Matsumoto E, Yoshida T, Kawarada Y, Sakakura T. Expression of fibronectin isoforms in human breast tissue: production of extra domain A+/extra domain B+ by cancer cells and extra domain A+ by stromal cells. *Jpn J Cancer Res*. 1999;90(3):320–325. doi:10.1111/j.1349-7006.1999.tb00750.x
26. Gould VE, Koukoulis GK, Virtanen I. Extracellular matrix proteins and their receptors in the normal, hyperplastic and neoplastic breast. *Cell Differ Dev*. 1990;32(3):409–416. doi:10.1016/0922-3371(90)90057-4
27. Korba BE, Wells FV, Baldwin B, et al. Hepatocellular carcinoma in woodchuck hepatitis virus-infected woodchucks: presence of viral DNA in tumor tissue from chronic carriers and animals serologically recovered from acute infections. *Hepatology*. 1989;9(3):461–470.

28. Midulla M, Verma R, Pignatelli M, Ritter MA, Courtenay-Luck NS, George AJ. Source of oncofetal ED-B-containing fibronectin: implications of production by both tumor and endothelial cells. *Cancer Res*. 2000;60(1):164–169.
29. Salem N, Kuang Y, Wang F, Maclennan GT, Lee Z. PET imaging of hepatocellular carcinoma with 2-deoxy-2[18F]fluoro-D-glucose, 6-deoxy-6 [18F] fluoro-D-glucose, [1-11C]-acetate and [N-methyl-11C]-choline. *Q J Nucl Med Mol Imaging*. 2009;53(2):144–156.
30. Kuang Y, Salem N, Tian H, et al. Imaging lipid synthesis in hepatocellular carcinoma with [methyl-11c]choline: correlation with in vivo metabolic studies. *J Nucl Med*. 2011;52(1):98–106. doi:10.2967/jnumed.110.080366
31. Salem N, Kuang Y, Corn D, et al. [(Methyl)1-(11)c]-acetate metabolism in hepatocellular carcinoma. *Mol Imaging Biol*. 2011;13(1):140–151. doi:10.1007/s11307-010-0308-y
32. Kuang Y, Wang F, Corn DJ, Tian H, Lee Z. Metabolism of radiolabeled methionine in hepatocellular carcinoma. *Mol Imaging Biol*. 2014;16 (1):44–52. doi:10.1007/s11307-013-0678-z
33. Kolthammer JA, Corn DJ, Tenley N, et al. PET imaging of hepatocellular carcinoma with 18F-fluoroethylcholine and 11C-choline. *Eur J Nucl Med Mol Imaging*. 2011;38(7):1248–1256. doi:10.1007/s00259-011-1743-y
34. Kuang Y, Salem N, Corn DJ, et al. Transport and metabolism of radiolabeled choline in hepatocellular carcinoma. *Mol Pharm*. 2010;7 (6):2077–2092. doi:10.1021/mp1001922
35. Kuang Y, Salem N, Wang F, Schomisch SJ, Chandramouli V, Lee Z. A colorimetric assay method to measure acetyl-CoA synthetase activity: application to woodchuck model of hepatitis virus-induced hepatocellular carcinoma. *J Biochem Biophys Methods*. 2007;70(4):649–655. doi:10.1016/j.jbbm.2007.02.008
36. Kuang Y, Schomisch SJ, Chandramouli V, Lee Z. Hexokinase and glucose-6-phosphatase activity in woodchuck model of hepatitis virus-induced hepatocellular carcinoma. *Comp Biochem Physiol C Toxicol Pharmacol*. 2006;143(2):225–231. doi:10.1016/j.cbpc.2006.02.005
37. Kuang Y, Wang F, Corn DJ, Tian H, Lee Z. In vitro characterization of uptake mechanism of L-[methyl-(3)H]-methionine in hepatocellular carcinoma. *Mol Imaging Biol*. 2014;16(4):459–468. doi:10.1007/s11307-014-0720-9
38. Salem N, MacLennan GT, Kuang Y, et al. Quantitative evaluation of 2-deoxy-2[F-18]fluoro-D-glucose-positron emission tomography imaging on the woodchuck model of hepatocellular carcinoma with histological correlation. *Mol Imaging Biol*. 2007;9(3):135–143. doi:10.1007/s11307-007-0092-5
39. Andres Ibarra R, Abbas R, Kombu RS, et al. Disturbances in the glutathione/ophthalmate redox buffer system in the woodchuck model of hepatitis virus-induced hepatocellular carcinoma. *HPB Surg*. 2011;2011:789323. doi:10.1155/2011/789323
40. Gerin JL, Cote PJ, Korba BE, Tennant BC. Hepadnavirus-induced liver cancer in woodchucks. *Cancer Detect Prev*. 1989;14(2):227–229.
41. Love MI, Huber W, Anders S. Moderated estimation of fold change and dispersion for RNA-seq data with DESeq2. *Genome Biol*. 2014;15(12):550. doi:10.1186/s13059-014-0550-8
42. Fletcher SP, Chin DJ, Ji Y, et al. Transcriptomic analysis of the woodchuck model of chronic hepatitis B. *Hepatology*. 2012;56(3):820–830. doi:10.1002/hep.25730
43. Han Z, Li Y, Roelle S, et al. Targeted contrast agent specific to an oncoprotein in tumor microenvironment with the potential for detection and risk stratification of prostate cancer with MRI. *Bioconjug Chem*. 2017;28(4):1031–1040. doi:10.1021/acs.bioconjchem.6b00719
44. Julyan PJ, Taylor JH, Hastings DL, Williams HA, Zweit J. SUVpeak: a new parameter for quantification of uptake in FDG PET. *Nucl Med Commun*. 2004;25(4):407. doi:10.1097/00006231-200404000-00040
45. Wahl RL, Jacene H, Kasamon Y, Lodge MA. From RECIST to PERCIST: evolving Considerations for PET response criteria in solid tumors. *J Nucl Med*. 2009;50(Suppl 1):122S–50S. doi:10.2967/jnumed.108.057307
46. Scarpino S, Stoppacciaro A, Pellegrini C, et al. Expression of EDA/EDB isoforms of fibronectin in papillary carcinoma of the thyroid. *J Pathol*. 1999;188(2):163–167. doi:10.1002/(SICI)1096-9896(199906)188:2<163::AID-PATH335>3.0.CO;2-1
47. Attieh Y, Clark AG, Grass C, et al. Cancer-associated fibroblasts lead tumor invasion through integrin-beta3-dependent fibronectin assembly. *J Cell Biol*. 2017;216(11):3509–3520. doi:10.1083/jcb.201702033
48. Erdogan B, Ao M, White LM, et al. Cancer-associated fibroblasts promote directional cancer cell migration by aligning fibronectin. *J Cell Biol*. 2017;216(11):3799–3816. doi:10.1083/jcb.201704053
49. Mhawech-Fauceglia P, Wang D, Samrao D, et al. Clinical implications of marker expression of carcinoma-associated fibroblasts (CAFs) in patients with epithelial ovarian carcinoma after treatment with neoadjuvant chemotherapy. *Cancer Microenvir*. 2014;7(1–2):33–39. doi:10.1007/s12307-013-0140-4
50. Conte GD, Tosi D, Fasolo A, et al. A Phase I trial of antifibronecitin 131I-L19-small immunoprotein (L19-SIP) in solid tumors and lymphoproliferative disease. *J Clin Oncol*. 2008;26(15_suppl):2575. doi:10.1200/jco.2008.26.15_suppl.2575
51. Berndorff D, Borkowski S, Moosmayer D, et al. Imaging of tumor angiogenesis using 99mTc-labeled human recombinant anti-ED-B fibronectin antibody fragments. *J Nucl Med*. 2006;47(10):1707–1716.
52. Trott O, Olson AJ. AutoDock Vina: improving the speed and accuracy of docking with a new scoring function, efficient optimization, and multithreading. *J Comput Chem*. 2010;31(2):455–461. doi:10.1002/jcc.21334
53. Giesel FL, Kratochwil C, Lindner T, et al. (68)Ga-FAPI PET/CT: biodistribution and preliminary dosimetry estimate of 2 DOTA-containing FAP-targeting agents in patients with various cancers. *J Nucl Med*. 2019;60(3):386–392. doi:10.2967/jnumed.118.215913
54. Kratochwil C, Flechsig P, Lindner T, et al. (68)Ga-FAPI PET/CT: tracer uptake in 28 different kinds of cancer. *J Nucl Med*. 2019;60(6):801–805. doi:10.2967/jnumed.119.227967
55. Chayanupatkul M, Omino R, Mittal S, et al. Hepatocellular carcinoma in the absence of cirrhosis in patients with chronic hepatitis B virus infection. *J Hepatol*. 2017;66(2):355–362. doi:10.1016/j.jhep.2016.09.013
56. Tennant BC, Toshkov IA, Peek SF, et al. Hepatocellular carcinoma in the woodchuck model of hepatitis B virus infection. *Gastroenterology*. 2004;127(5 Suppl 1):S283–S293. doi:10.1053/j.gastro.2004.09.043